

Climate sensitivity constrained by temperature reconstructions over the past seven centuries

Gabriele C. Hegerl¹, Thomas J. Crowley¹, William T. Hyde¹ & David J. Frame²

The magnitude and impact of future global warming depends on the sensitivity of the climate system to changes in greenhouse gas concentrations. The commonly accepted range for the equilibrium global mean temperature change in response to a doubling of the atmospheric carbon dioxide concentration¹, termed climate sensitivity, is 1.5–4.5 K (ref. 2). A number of observational studies^{3–10}, however, find a substantial probability of significantly higher sensitivities, yielding upper limits on climate sensitivity of 7.7 K to above 9 K (refs 3–8). Here we demonstrate that such observational estimates of climate sensitivity can be tightened if reconstructions of Northern Hemisphere temperature over the past several centuries are considered. We use large-ensemble energy balance modelling and simulate the temperature response to past solar, volcanic and greenhouse gas forcing to determine which climate sensitivities yield simulations that are in agreement with proxy reconstructions. After accounting for the uncertainty in reconstructions and estimates of past external forcing, we find an independent estimate of climate sensitivity that is very similar to those from instrumental data. If the latter are combined with the result from all proxy reconstructions, then the 5–95 per cent range shrinks to 1.5–6.2 K, thus substantially reducing the probability of very high climate sensitivity.

We use four palaeoreconstructions, namely a hemispheric reconstruction of mean annual temperatures¹¹, a maximum latewood density tree ring based reconstruction¹² for growing season temperatures over 20–90° N land, a revised and smoothed version of a record¹³ that has been calibrated to 30–90° N land annual data¹⁴, and our own new decadal reconstruction termed ‘CH-blend’ of annual average 30–90° N temperature¹⁵ (Fig. 1). A version of CH-blend using 12 records extends from AD 1505 to AD 1960; and a reconstruction based on 9 sites (‘CH-blend (long)’) is used from AD 1270. Both reconstructions use a relatively small number of well spaced sites (often based on multiple records, including some regional reconstructions) throughout the reconstruction. CH-blend is consistent with independent estimates of temperatures from boreholes¹⁵, and both CH-blend and CH-blend (long) agree well with a recent reconstruction¹⁶ that incorporates records of lower temporal resolution. The reconstruction method has been tested using noise-perturbed climate model data from the same locations as used in the reconstruction¹⁵. Results show that the reconstruction of decadal temperatures is accurate and reliably preserves the variance of hemispheric-scale temperature variability.

For CH-blend, our estimate of climate sensitivity fully accounts for the uncertainty in the amplitude of the record¹⁵. For the other reconstructions, we use both the published reconstruction and a version that is recalibrated using our technique. This approach avoids introducing a low bias in our estimate of climate sensitivity based on the possibility that some reconstruction

techniques underestimate past climate variability¹⁷ (for details see Supplementary Information).

We conduct a large ensemble (>1,000) of simulations of the past 1,000 years with a 2.5-dimensional (latitude/longitude/depth) upwelling-diffusion energy balance model (EBM), with realistic land-sea distribution. The EBM is a variant of a seasonal model¹⁸ that simulates time-dependent responses to external forcing, and includes the seasonal cycle (for details see Supplementary Information). The same model has been previously used to examine the relationship between reconstructed temperature and external forcing over the past millennium^{19,20}. EBM simulations reproduce the large-scale temperature response of general circulation models, and have the advantage of being able to generate large ensembles.

The following two model parameters are important determinants of the large-scale response of climate models to external forcing⁵ and have been systematically varied in our ensemble. First, the equilibrium climate sensitivity to a doubling of CO₂, α , which was varied in 0.5 K increments from 0.5 K to 10.0 K with an additional low value of 0.25 K. Second, effective ocean diffusivity κ in the upwelling-diffusive model²¹, which was varied between 0.63 cm² s⁻¹ and 3.8 cm² s⁻¹.

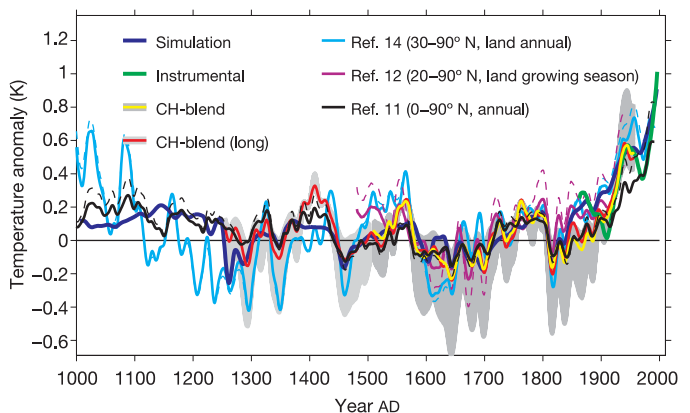


Figure 1 | Palaeoclimatic records compared to a climate model simulation. ‘CH-blend’ and ‘CH-blend (long)’ represent 30–90° N annual mean temperature (grey shading shows 10–90% ranges for uncertainty in the amplitude of the reconstruction); ref. 11 shows 0–90° N land temperature; ref. 14 shows 30–90° N land temperature; and ref. 12 shows 20–90° N land growing season temperature (dashed line indicates reconstructions rescaled¹⁵). The model (‘Simulation’) has a sensitivity of 2.5 K, mid-range ocean diffusivity and is driven with mid-range aerosol forcing. All data are smoothed to focus on multi-decadal variability and shown as anomalies relative to the period before 1800. The instrumental record for 30–90° N annual mean surface temperature (‘Instrumental’) is offset to match CH-blend between 1880 and 1960.

¹Division of Earth and Ocean Sciences, Nicholas School of the Environment and Earth Sciences, Duke University, Durham, North Carolina, 27708, USA. ²Climate Dynamics Group, Department of Physics, University of Oxford, Oxford OX1 3PU, UK.

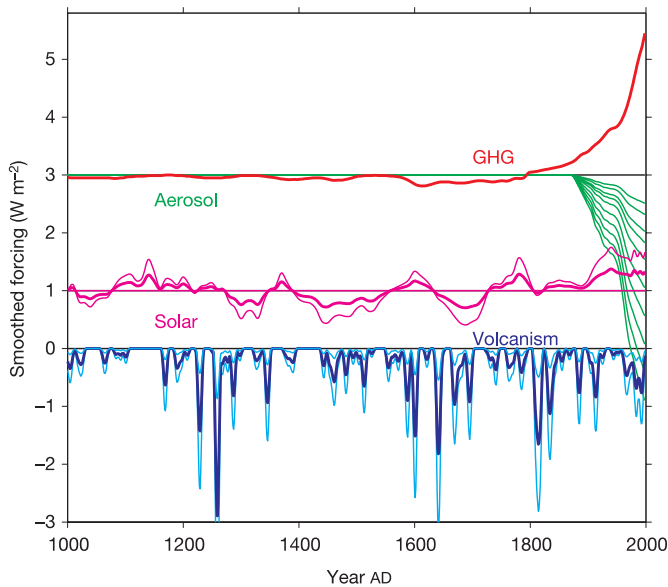


Figure 2 | Northern Hemisphere mean radiative forcing. Sub-annual forcing data are used in the climate model simulations, but a decadal filter is applied here for illustration only, to focus on timescales most relevant for the analysis. For tropospheric aerosol forcing (green), a range of forcing has been used; for solar (pink) and volcanic (blue) forcing, a best guess forcing (dark, thick line) and a gaussian uncertainty range has been used (2.5% and 97.5% limits are shown by light, thin lines, the lower limit for solar is on the zero line). For clarity, greenhouse gas ('GHG') and aerosol forcings are offset by 3 W m^{-2} , and solar forcing by 1 W m^{-2} .

This range embraces an observational estimate of $1.7 \pm 0.2 \text{ cm}^2 \text{ s}^{-1}$ based on a global compilation of GEOSCECS data of bomb tritium penetration into the world ocean²² and a lower range²³ based on bomb ^{14}C of the order of $1 \text{ cm}^2 \text{ s}^{-1}$. We have further tested our range of diffusivities by comparing simulated ocean warming with ocean heat content data²⁴. We find that the smaller to mid-range values of κ yield results that compare most favourably with these data, consistent with the observation that most of the twentieth-century increase in ocean heat content is in the upper 1,000 m (Supplementary Fig. 1). Note that ocean diffusivity is of smaller importance for the simulations of the pre-industrial period, where forcings are mostly episodic and relatively small, than for the twentieth century. In the latter period, the rate of temperature increase is crucially influenced by ocean diffusivity, as large diffusivities tend to hide more warming

in the oceans than small diffusivities (see Supplementary Information for more discussion). Our results are insensitive to attempts to constrain κ further. They are, however, conditional on ocean effective diffusivity being within the range we use.

Prior work^{15,19,20,25} has established that various reconstructions of hemispheric temperature consistently show influence from volcanic and greenhouse gas variations, and less consistently from variations in solar radiation. We force the EBM simulations with a combination of solar, volcanic, greenhouse gas and tropospheric aerosol forcing to simulate hemispheric temperature change over the past millennium (Fig. 2). Greenhouse gas forcing is based on changes in trace gases from ice-core data, combined with IPCC estimates of radiative forcing for well-mixed greenhouse gases in the twentieth century. The estimate of solar forcing is based on ^{14}C data²⁶, scaled to the solar irradiance reconstruction of ref. 27 after reducing its amplitude by 20% to accommodate recent conclusions that the former estimate may have been large²⁸. For volcanism, we use an update of a global reconstruction²⁰ based on ice-core data from Greenland and Antarctica. We account for the considerable uncertainty in solar and volcanic forcing by varying the total amplitude of each forcing time-series around its central estimate. We use Monte Carlo simulations based on a 50% standard deviation for solar forcing, and a 35% standard deviation for volcanic forcing (excluding the unphysical case of net negative forcing). The uncertainty in our results due to random errors in the magnitude of individual volcanic eruptions was estimated by sensitivity tests, indicating that errors in the magnitude of individual eruptions can cause a modest widening of the tail of the distribution (Supplementary Fig. 2; see Supplementary Information for more detail on forcings and their uncertainty).

We derive a probability density function (PDF) for climate sensitivity using a method related to one previously used for instrumental data^{5,6} (see Methods section, and algorithm in Supplementary Information). Results for the CH-blend reconstruction, for which we have the most reliable uncertainty estimate¹⁵, yield a 5–95% range for sensitivity of 1.4 K to 6.1 K and a median sensitivity of 2.6 K over the pre-instrumental period 1505–1850 (Fig. 3a). PDFs for climate sensitivity from the other reconstructions and the same period yield peak probabilities (modes) from 1.3 K to 3.6 K, and some of them suggest a moderate probability for climate sensitivity being high (see Supplementary Table 4). Reconstructions with higher amplitudes of past climate fluctuations generally suggest higher climate sensitivities than those with low variability. The range of the other free parameters, ocean diffusivity κ , and solar and volcanic forcing uncertainty, are used to fully explore uncertainties rather than to provide posterior information about best-fit values.

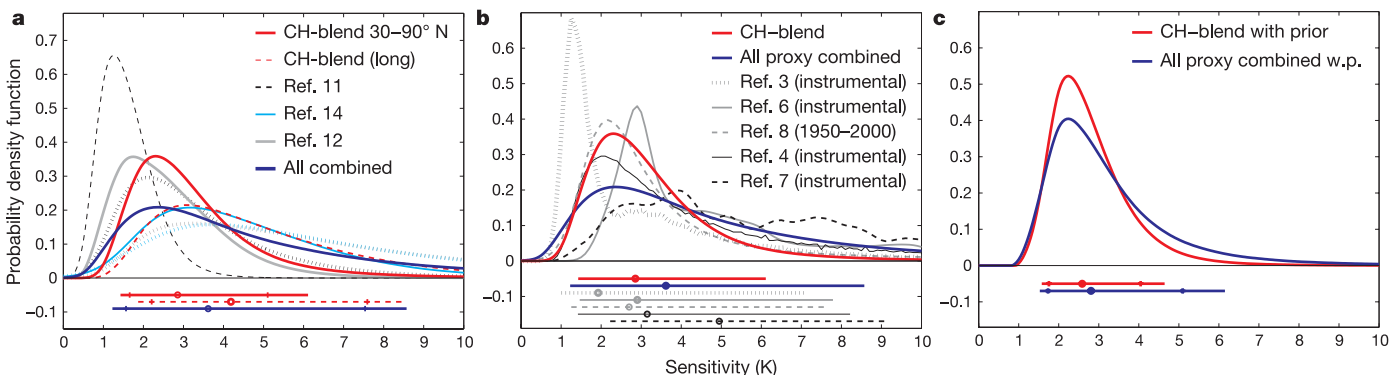


Figure 3 | Estimated probability density functions (PDFs) for equilibrium climate sensitivity to CO_2 doubling (in K). **a**, PDFs from a range of palaeoreconstructions using data to 1850 (dotted lines, based on rescaled data). The horizontal bars indicate the 5–95% range of PDFs (median is indicated by a dot, and 10th and 90th percentiles by a vertical bar).

b, Comparison to other estimates of climate sensitivity based on instrumental data^{3,4,6,7} over the twentieth century or 1950–2000⁸. All PDFs have been scaled to integrate to 1 between 0 and 10 for better comparison. **c**, Combined estimate using a result from instrumental data³ as prior distribution, updated by the result from pre-industrial data ('w.p.').

Consistent with that, the pre-industrial period does not provide constraints for ocean diffusivity, nor do results consistently favour a particular realization of forcing uncertainty, apart from a general preference for solar forcing on the low end of the range.

If all four reconstructions, both published and rescaled, are considered as equally likely realizations of the true hemispheric temperature evolution, the PDF that describes results from all four reconstructions combined yields a median sensitivity of 3.4 K and a 5–95% range of 1.2 K to 8.6 K. This renders negative climate feedbacks to CO₂ changes (corresponding to a climate sensitivity of under 1.1 K) very unlikely. As in other estimates of climate sensitivity, the upper tail is not well constrained. Note that the upper limit of the transient climate response, which governs the near-term magnitude of the climate response, tends to be better constrained from observations than equilibrium climate sensitivity⁸.

Our results are remarkably consistent with PDFs for climate sensitivity that have been estimated from the instrumental record^{13–8} (Fig. 3b) and that account for a differing level of uncertainty in forcings (most notably aerosol forcing⁷), ocean diffusivity and observations. The response of climate to pre-industrial forcing is governed (to a very reasonable approximation) by the same climate sensitivity. However, the uncertainties affecting each estimate are virtually independent, as the pre-industrial temperature reconstructions are virtually independent from instrumental temperatures for the second half of the twentieth century (decadal data before that are used for calibrating the palaeodata) and different forcing uncertainties affect each estimate. Therefore we can combine results from both to further constrain sensitivity. We use a version of the joint PDF for diffusivity and sensitivity, κ and α , from ref. 8 that is based on decadal instrumental data from 1950 to 2000 as a prior probability distribution (the use of a prior PDF of κ and α combined accounts for their dependence; Supplementary Fig. 5 shows a comparison between the published results for the entire twentieth century⁸ and the prior used here). We have widened the upper tail of the ref. 8 estimate in sensitivity in order to conservatively account for further uncertainties and embrace other instrumental estimates (results are only moderately sensitive to this, for details see Supplementary Information). Bayes' theorem is then used to calculate a posterior probability based on data from the past millennium (Fig. 3c). The resulting 5–95% ranges for CH-blend shrink to 1.6 K to 4.6 K, and those for all proxy data combined to 1.5 K to 6.2 K. This result reduces the probability from 36% to 15% or less that climate sensitivity exceeds the upper limit of the IPCC range of 4.5 K.

As previously shown, the agreement between models and data is mostly driven by the temperature response to volcanism, which causes longer-term variability due to the changing statistics of volcanic eruptions (Fig. 2; see also Supplementary Table 3 for correlations between simulations and records on short and long timescales). A superposed epoch analysis previously showed that the EBM simulates the response-characteristics to volcanism very well¹⁹. The EBM does not simulate changes in atmospheric dynamics that have been associated with strong volcanic eruptions²⁹, but these changes do not much affect hemispheric annually (or growing season) averaged temperatures³⁰.

We also note that model uncertainties (beyond those that we account for) potentially affect all estimates of climate sensitivity. Although our results are conditional on the range of effective ocean diffusivity and the upwelling parameter being realistic, simulated ocean heat content changes in our best-fit simulation compare very well with recent data²⁴ (Supplementary Fig. 1). A simulation with the most likely sensitivity of 2.5 K also compares well to the low-frequency component of annual global temperatures from instrumental data (Supplementary Fig. 4).

We conclude that proxy-reconstructions of the pre-industrial period from 1270 to 1850 yield very similar estimates of climate sensitivity to those obtained from the virtually independent climate change over the twentieth century. This agreement increases our

confidence in the overall reliability of these estimates based on twentieth-century changes. When both independent lines of evidence are combined, the resulting PDF for climate sensitivity narrows, yielding a very small probability for climate sensitivity exceeding 7 K (<3% based on all reconstructions combined, and <1% based on CH-blend).

METHODS

Estimating climate sensitivity. Our method of estimating the PDF of equilibrium climate sensitivity is related to a method used previously for instrumental data^{5,6} and is briefly discussed here. A detailed algorithm can be found in the Supplementary Information. We simulate the time-space evolution of surface temperature over the past millennium forced with observed changes in solar, volcanic, greenhouse gas and sulphate aerosol forcing. We use a very large ensemble of EBM simulations with varying climate sensitivity α and ocean diffusivity κ , forced by different realizations of solar and volcanic forcing (f_{sol} , f_{vol}) to account for the most important uncertain parameters driving the simulated response. For the twentieth century, aerosol forcing, f_{aer} , is also varied. Each model simulation yields a time-space pattern of surface temperature response for each parameter $T(x, t, \alpha, \kappa, f_{\text{sol}}, f_{\text{vol}}, f_{\text{aer}})$ that depends on time t and space x . For each palaeoreconstruction \bar{T}_{palaeo} (overbar denoting a spatial average), the simulated spatial temperature patterns are averaged over the latitude strip and season the reconstruction is calibrated to, and filtered to the time-resolution used for the analysis (annual reconstructions are filtered by a 5-yr running mean). All data are then centred from the beginning of the record to 1800 to focus on deviations from a mean climatic state of the past millennium and to avoid major variations in the climate state caused by anthropogenic forcing. We analyse reconstructions from the beginning of the record, but not before AD 1270 (as there are significant uncertainties in the radiative forcing effects of a very large eruption in 1258). The analysis focuses on the residual between the simulated record \bar{T} and the observed record:

$$\text{res}(t, \alpha, \kappa, f_{\text{sol}}, f_{\text{vol}}, f_{\text{aer}}) = \bar{T}_{\text{palaeo}}(t) - \bar{T}(t, \alpha, \kappa, f_{\text{sol}}, f_{\text{vol}}, f_{\text{aer}}) \quad (1)$$

Some combination of parameters will yield the residual with the smallest estimated variance, $\hat{\sigma}_{\text{min}}^2 = \min_{\text{parameters}} \left(\frac{\|\text{res}(t, \alpha, \kappa, f_{\text{sol}}, f_{\text{vol}}, f_{\text{aer}})\|^2}{n-1} \right)$, with $\|\text{res}\|^2 = \sum \text{res}(t, \alpha, \kappa, f_{\text{sol}}, f_{\text{vol}}, f_{\text{aer}})^2$ and n denoting the length of the residual time series (yr). The difference between any square residual $\|\text{res}\|^2$ and the minimum square residual $\|\text{res}_{\text{min}}\|^2$ will then be F-distributed⁵

$$\frac{\|\text{res}(\alpha, \kappa, f_{\text{aer}}, f_{\text{sol}}, f_{\text{vol}})\|^2 - \|\text{res}_{\text{min}}\|^2}{\hat{\sigma}_{\text{min}}^2} \propto mF(m, \nu) \quad (2)$$

where m is the number of free parameters (4 for the pre-industrial case, 5 for the entire time-series) and ν is the number of degrees of freedom in res_{min} . Note that for autocorrelated data, ν will be smaller than n . Therefore we account for the number of effectively independent samples in the square residual (see Supplementary Information). Thus, the likelihood of the reconstruction given each set of model parameters and forcings $p(\text{data}|\alpha, \kappa, f_{\text{aer}}, f_{\text{vol}}, f_{\text{sol}})$ is estimated from the probability that its residual variability is statistically indistinguishable from the best-fit residual⁵, given internal climate variability and non-climatic random errors in proxy data.

Bayes' theorem is used to derive the joint PDF of the parameters

$$p(\alpha, \kappa, f_{\text{aer}}, f_{\text{vol}}, f_{\text{sol}}|\text{data}) \propto p(\text{data}|\alpha, \kappa, f_{\text{aer}}, f_{\text{vol}}, f_{\text{sol}}) \cdot p(\alpha, \kappa, f_{\text{aer}}, f_{\text{vol}}, f_{\text{sol}}) \quad (3)$$

from the likelihood of the data and the prior probability of the parameters $p(\alpha, \kappa, f_{\text{aer}}, f_{\text{vol}}, f_{\text{sol}})$. For results based on the proxy data alone, a uniform prior distribution for α is used for integration, which extends to a sensitivity of 10 K and then drops off to zero. Similarly, a prior for κ is used that is uniform over the range we cover (see main text), and normal prior distributions are used for solar and volcanic uncertainty (see Fig. 2). Where a prior distribution from the late twentieth century is used, the joint probability density function $p(\alpha, \kappa)$ from ref. 8 is applied instead of the uniform distribution.

This analysis is performed for every reconstruction. For reconstructions where the amplitude uncertainty can be fully accounted for (CH-blend and CH-blend (long)), this analysis is performed for the reconstruction scaled by a range of scaling factors β , representing uncertainty in the amplitude of the reconstruction (see Supplementary Information). We use the best-guess scaling and the 2.5th, 10th, 25th, 75th, 90th and 97.5th percentile of β . All PDFs resulting from these analyses $p(\text{data}(\beta)|\alpha, \kappa, f_{\text{aer}}, f_{\text{vol}}, f_{\text{sol}})$ are then averaged over β , weighted by the likelihood of each scaling β based on a normal distribution. This is a robust way of incorporating uncertainty in the reconstruction, as random errors in the reconstruction are directly accounted for in the residual.

For reconstructions where the amplitude uncertainty cannot be fully estimated, we use both the published best guess and a rescaled best guess using our calibration method to estimate $p(\text{data}|\alpha, \kappa, f_{\text{aer}}, f_{\text{vol}}, f_{\text{sol}})$.

The resulting multi-dimensional likelihood is integrated over κ and forcing uncertainties $f_{\text{sol}}, f_{\text{vol}}$ and f_{aer} , yielding a PDF for climate sensitivity. This is done both for each reconstruction individually, and for the average of the joint probabilities $p(\alpha, \kappa, f_{\text{aer}}, f_{\text{vol}}, f_{\text{sol}}|\text{data})$ from all reconstructions to derive an estimate of climate sensitivity from all records combined.

Our method to estimate sensitivity has been validated using synthetic data (see Supplementary Fig. 2), and tested by using an alternative method to estimate the likelihood based on scaling factors (see Supplementary Information).

Received 8 July 2005; accepted 28 February 2006.

- Schneider, S. H. & Dickinson, R. E. Climate modeling. *Rev. Geophys. Space Phys.* **12**, 447–493 (1974).
- Cubasch, U., et al. in *Climate Change 2001: The Scientific Basis* (eds Houghton, J. T. et al.) 525–582 (Cambridge Univ. Press, New York, 2001).
- Andronova, N. G. & Schlesinger, M. E. Causes of global temperature changes during the 19th and 20th centuries. *Geophys. Res. Lett.* **27**, 2137–2140 (2000).
- Gregory, J. M., Stouffer, R. J., Raper, S. C., Stott, P. A. & Rayner, N. A. An observationally based estimate of the climate sensitivity. *J. Clim.* **15**, 3117–3121 (2002).
- Forest, C. E., Stone, P. H., Sokolov, A. P., Allen, M. R. & Webster, M. D. Quantifying uncertainties in climate system properties with the use of recent observations. *Science* **295**, 113–117 (2002).
- Forest, C. E., Stone, P. H. & Sokolov, A. P. Estimated PDFs of climate system properties including natural and anthropogenic forcings. *Geophys. Res. Lett.* (in the press).
- Knutti, R., Stocker, T. F., Joos, F. & Plattner, G.-K. Constraints on radiative forcing and future climate change from observations and climate model ensembles. *Nature* **416**, 719–723 (2002).
- Frame, D. J. et al. Constraining climate forecasts: The role of prior assumptions. *Geophys. Res. Lett.* **32**, L09702, doi:10.1029/2004GL0022241 (2005).
- Murphy, J. M. et al. Quantification of modelling uncertainties in a large ensemble of climate change simulations. *Nature* **430**, 768–772 (2004).
- Stainforth, D. A. et al. Uncertainty in predictions of the climate response to rising levels of greenhouse gases. *Nature* **433**, 403–406 (2005).
- Mann, M. E. & Jones, P. D. Global surface temperatures over the past two millennia. *Geophys. Res. Lett.* **30**, 1820, doi:10.1029/2003GL017814 (2003).
- Briiffa, K. R. et al. Low-frequency temperature variations from a northern tree ring density network. *J. Geophys. Res.* **106**, 2929–2941 (2001).
- Esper, J., Cook, E. R. & Schweingruber, F. Low-frequency signals in long tree-ring chronologies for reconstructing past temperature variability. *Science* **295**, 2250–2253 (2002).
- Cook, E., Esper, J. & D'Arrigo, R. Extra-tropical Northern Hemisphere land temperature variability over the past 1000 years. *Quat. Sci. Rev.* **23**, 2063–2074 (2004).
- Hegerl, G. C. et al. Detection of human influence on a new, validated 1500 yr temperature reconstruction. *J. Clim.* (submitted).
- Moberg, A., Sonechkin, D. M., Holmgren, K., Datsenko, N. M. & Karlen, W. Highly variable Northern Hemisphere temperatures reconstructed from low- and high-resolution proxy data. *Nature* **433**, 613–617 (2005).
- von Storch, H. et al. Reconstructing past climate from noisy data. *Science* **306**, 679–682 (2004).
- North, G. R., Mengel, J. G. & Short, D. A simple energy balance model resolving the seasons and continents: Application to the astronomical theory of the ice ages. *J. Geophys. Res.* **88**, 6576–6586 (1983).
- Hegerl, G. C., Crowley, T. J., Baum, S. K., Kim, K.-Y. & Hyde, W. T. Detection of volcanic, solar, and greenhouse gas signals in paleo-reconstructions of Northern Hemispheric temperature. *Geophys. Res. Lett.* **30**, 1242, doi:10.1029/2002GL016635 (2003).
- Crowley, T. J., Baum, S. K., Kim, K.-Y., Hegerl, G. C. & Hyde, W. T. Modeling ocean heat content changes during the last millennium. *Geophys. Res. Lett.* **30**, 1932, doi:10.1029/2003GL017801 (2003).
- Crowley, T. J. & Kim, K.-Y. Modeling the temperature response to forced climate change over the last six centuries. *Geophys. Res. Lett.* **26**, 1901–1904 (1999).
- Li, Y.-H., Peng, T.-H., Broecker, W. S. & Oestlund, H. G. The average vertical mixing coefficient for the oceanic thermocline. *Tellus B* **36**, 212–217 (1984).
- Siegenthaler, U. Uptake of excess CO₂ by an outcrop-diffusion model of the ocean. *J. Geophys. Res.* **88**, 3599–3608 (1983).
- Levitus, S., Antonov, J. & Boyer, T. Warming of the world ocean, 1955–2003. *Geophys. Res. Lett.* **32**, L02604, doi:10.1029/2004GL021592 (2005).
- Free, M. & Robock, A. Global warming in the context of the little Ice Age. *J. Geophys. Res.* **104**, 19057–19070 (1999).
- Stuiver, M. & Braziunas, T. F. Modeling atmospheric ¹⁴C influence and ¹⁴C ages of marine samples to 10,000 BC. *Radiocarbon* **35**, 137–189 (1993).
- Lean, J. L., Beer, J. & Bradley, R. Reconstruction of solar irradiance changes since 1610: Implications for climate change. *Geophys. Res. Lett.* **22**, 3195–3198 (1995).
- Lean, J. L., Wang, Y.-M. & Sheeley, N. R. The effect of increasing solar activity on the Sun's total open magnetic flux during multiple cycles: Implications for solar forcing of climate. *Geophys. Res. Lett.* **29**, 2224, doi:10.1029/2002GL015880 (2002).
- Shindell, D. T., Schmidt, G. A., Mann, M. E. & Faluvegi, G. Dynamic winter climate response to large tropical volcanic eruptions since 1600. *J. Geophys. Res.* **109**, D05104, doi:10.1029/2003JD004151 (2004).
- Thompson, D., Wallace, J. M. & Hegerl, G. C. Annular modes in the extratropical circulation: Part II, Trends. *J. Clim.* **13**, 1018–1036 (2000).

Supplementary Information is linked to the online version of the paper at www.nature.com/nature.

Acknowledgements We thank C. Forest for suggesting merging PDF estimates from results based on past-millennium climate changes with those based on twentieth-century climate change; J. Kenyon for technical support; M. Allen, F. Zwiers, A. Gelfand and M. Lavine for discussions; and C. Forest, N. Andronova, R. Knutti and J. Gregory for providing data. G.C.H. and T.J.C. were supported by NOAA, NOAA's office of global programmes and the DOE's office of biological and environmental research. G.C.H. was additionally supported by NSF.

Author Contributions G.C.H. developed and implemented the method to estimate sensitivity and to calibrate proxy records, T.J.C. provided the reconstruction of past forcing and developed the CH-blend reconstruction, W.T.H. performed the EBM simulation, and D.J.F. derived the prior estimate of sensitivity from instrumental data 1950–2000. G.C.H., T.J.C. and W.T.H. analysed the results.

Author Information Reprints and permissions information is available at npg.nature.com/reprintsandpermissions. The authors declare no competing financial interests. Correspondence and requests for materials should be addressed to G.C.H. (hegerl@duke.edu).